Trajectory estimation model for a solid body with an irregular shape undergoing extremely high aerodynamic forces

Elvedin Kljuno[1], Alan Catovic[2]

[1] Mechanical Engineering Faculty, University of Sarajevo, Bosnia and Herzegovina, e-mail: kljuno@mef.unsa.ba
[2] Mechanical Engineering Faculty, University of Sarajevo, Bosnia and Herzegovina, e-mail: catovic@mef.unsa.ba

ABSTRACT

A generalized (6DOF) model for evaluating fragment trajectory elements is defined, which incorporates a novel model for estimating the projected surface of the body and novel model for estimating aerodynamic force and moment. This 6DOF model is developed on the basis of differential equations of the center of mass motion and movement around the center of mass (currently no known model incorporates movement of the body around its center of mass), and can model the parameters that play an essential role in movement of the bodies with irregular shape through the atmosphere. In our model the basic parameters (i.e. body dimensions) can be arbitrarily changed in the initial part of the analysis, and based on their values and values of initial kinematic parameters (initial velocity, position, orientation), trajectories can be determined (as well as other parameters: velocities, orientation) in a relatively short amount of time.

The calculation of the complete trajectory of the fragments can be used in a number of applications: the analysis of the effects of the fragments (i.e. the safety analysis of the location of the ammunition depots, due to the potential explosion of the projectile) or in the estimation of a danger zones when demining larger quantities of the munition. Also, from the point of view of the parameters of the lethal zone of HE projectiles, it is generally important to estimate the trajectory of the fragments in the range up to 50m, so this model can be used to model such a scenario also. This model could also be potentially used wherever there is a need to calculate flight mechanics parameters of irregularly shaped bodies.

Generalized (6DOF) model for estimation of an irregularly shaped body trajectory is implemented in a computer program, written in MatLab. Based on the model, the trajectory calculations were performed for the complete trajectory and for shorter distances to the center of the explosion, with varied geometric-inertial parameters and initial kinematic conditions for the given fragment.

Keywords: Aerodynamic force, Irregular shape, Fragment, Solid body, Trajectory

Corresponding Author:

Elvedin Kljuno

Vilsonovo setaliste 9
71000 Sarajevo, Bosnia
E-mail: kljuno@mef.unsa.ba

1. Introduction

Motion of irregular shape bodies at high velocities through the atmosphere is complex and generally difficult for analysis. Examples of such bodies include fragments of high explosive devices (projectiles, bombs, improvised explosive devices), shrapnel generated by fractures of various structures due to the effects of strong storms, meteoroids (smaller stones or metal bodies from the space), comets (icy bodies from the outer part of the solar system), asteroids (larger bodies of different structures that also come from the solar system).

While fragments of high explosive devices move at initial velocities of 2 to 6 Mach (dimensional quantity representing the ratio of flow velocity past a boundary to the local speed of sound), meteoroids, comets and

asteroids move at considerably higher velocities when entering the atmosphere (about 50 Mach and more). Irregular shape bodies that are moving with high velocities are characterized by viscous and compressible fluid flow, dominant resistance due to pressure drag, shock waves, turbulent flow, and by a significant separation of the boundary layer from the surface of the body during movement.

In military applications, prediction of the movement of fragments generated by detonation of HE missiles is important for estimating the projectile lethal zone, for estimating the spatial density of fragments, as well as for estimating the range of fragments needed to calculate the safe distance. In the literature [1, 2], various models of dynamics of primary fragments (created by projectile detonation) and secondary fragments (concrete, wood, metal and other types of fragments created as a secondary effect of explosive devices) are mentioned. These models are mostly 2-DOF (2 degrees of freedom) or 3-DOF models that consider only one component of the aerodynamic force – drag force ([3], [4]).

It has been found that for a large number of fragment shapes (such as plates, thin fragments or structural elements with high slenderness ratio), dynamics models mentioned (taking into account only the drag force) predict smaller fragment range than it is the case in reality. In addition, if there is a possibility of stabilization of fragments due to a potentially high angular velocity of the fragment, the safety distance from such fragments could be higher than for non-stable fragments [5].

Twisdale [1] mentions the RO (a random orientation) model that uses the drag force, lift force and side force, whereby the model simulates periodic reorientation of fragments (using random numbers selected from a uniform distribution on a unit interval) in space. This model is implemented in the computer code TORMIS [1] used for risk assessment of fragments created by the effects of severe storms (wind-borne debris hazards) and can also be used for primary and secondary fragments caused by explosions. The TORMIS program was not publicly available at the time of writing.

Twisdale [1] in his work states the TORMIS model uses cross-flow theory in order to (as a function of an attack and roll angles) analytically estimate the aerodynamic coefficients for a uniformly random spatial orientation of the body, knowing the aerodynamic coefficient values for precisely defined directions of the body of known geometry (approximation of the shape of the fragment by known geometric form – rectangular parallelepiped of different dimensions). Based on the value of the drag, lift and side force coefficients, and knowing the values of dynamic pressure and the reference area of the body (exposed area of a parallelepiped), a total aerodynamic force is estimated. A set of six coupled nonlinear differential equations is further numerically integrated to obtain elements of body trajectory. Twisdale also reports that an aerodynamic library for typical fragment shapes has been developed for use with the random orientation 6DOF model.

Hokanson [2] provides a brief overview of some of the models for the estimation of fragment trajectory. From his research [2] it can be concluded that some authors used (semi)empirical formulas for predicting the velocity and range of fragments. Thus Connor [6] gives in his paper the empirical expression for the range of fragments as a function of velocity. Hokanson report also expressions are given by Swisdak [7], in which the range is a function of the initial elevation angle of the fragment and the ratio of the free fall velocity of the fragment and its initial velocity.

In different references (e.g., [2]) one can find expressions for predicting the velocity of a fragment based on the assumption that the coefficient of aerodynamic drag is constant. Based on the same assumption, a simple analytical expression for the range can be used in fast estimates for the maximum range of fragments. Of course, this approximation (drag coefficient has a constant value) can significantly affect the range of fragments because the drag coefficient, in general, depends on the shape of the fragment and its velocity (Mach number). Schreyer and Romesberg [9] carried out basic differential equations for predicting the trajectory of fragments in the atmosphere, assuming that the gravitational force and the drag force act on the fragment. In their model, the drag coefficient was also constant.

The model with drag and lift force was incorporated into the FRISB model (steel fragments from the spherical and cylindrical high-pressure containers) developed by W. Baker [10] with associates. The system of differential equations describing the movement of the fragments in the atmosphere, used in the FRISB model, is obtained

by projecting forces acting on a body onto coordinates x and y [10]. Using FRISB model, Baker et al. [10] constructed a special set of curves for estimating the maximum range of fragments using the non - dimensional parameters involving velocity, range as well as lift and drag ratio. Thus, relatively fast one could "graphically" roughly estimate the range of fragments for certain initial parameters. For a more accurate analysis, the computer code of the FRISB model with differential equations was used, where numerical methods were used for calculation. In the FRISB model, the drag coefficient and the lift coefficient are constant. Baker does not state how these coefficients were obtained and for which conditions.

Recently, Murman et al. [11] used a CFD method for determining the aerodynamic characteristics (drag coefficients) of debris, shedding from the Space Shuttle Launch Vehicle. They used Cartesian fully-coupled, six-degree-of-freedom simulations of isolated debris pieces in a Monte Carlo fashion to produce models for the drag and cross-range behavior over a range of debris shapes and shedding scenarios. The geometry of a blunt body was specified with a CAD solid model, either from an analytic definition or from 3D digitized data.

Murman et al. [11] computed drag coefficients using several different simulation methods: static simulations (the body was held fixed with the minimum and maximum frontal area exposed to the wind respectively), "forced-tumble" simulation (the body was rotated at simulations over a complete cycle in order to simulate an "average" dynamic motion) and 6-DOF simulation (the body being released into a uniform stream and allowed to decelerate and rotate under the influence of the aerodynamic loads). The downside of this method is the large computer resource demands needed for such a procedure (Murman et al. [11] used clusters with 10240 processor for this task - NASA Ames Altix Supercomputer). Most of researchers do not have access to supercomputers (computers with large numbers of processors). Also, this method uses 3D CAD solid models of debris for each individual analysis, which can be impractical since every fragment is of different shape.

The model described in this paper is a parametrical model that can be used to very efficiently model the parameters which play an essential role in fragment dynamics during its motion through the atmosphere. This means that the basic parameters (in this case the fragment dimensions) can be arbitrarily changed in the initial part of the analysis and based on their values and values of the initial kinematic parameters (initial velocities, position, orientation), the trajectory of fragments (as well as other parameters: translational and angular velocities, stability, orientation) can be determined in a relatively short time.

Generally, after the review of the available literature, we found that there is currently no adequate model of flight mechanics for fragments (bodies) with an irregular shape that accurately calculates the movement of its center of mass and determines the orientation of the body at every moment, based on aerodynamic forces and moments acting on it. Some publicly available models are based on statistical methods, justifying their assumptions in a variety of ways. However, the statistical method cannot give precise results, and at most can indicate a certain trend in the phenomenology.

In addition, in most studies, aerodynamic coefficients are determined experimentally [17], analytically for arbitrary orientation or assumed constant. In our model, there is no need to calculate aerodynamic coefficients (which are generally used in other models to determine the forces and moments needed to calculate the trajectory) because the forces and moments are determined directly by approximating the irregular body surface and integrating the aerodynamic effect over the surface area, as shown in [15].

The third issue in (available) models of fragments dynamics is the evaluation of the reference area value that is required for the calculation of force. Here also, the statistical method is often introduced, simplifying the model and thereby reducing its accuracy. In the previous related work [14], on the other hand, the exposed area of the fragment (perpendicular to the velocity vector) is precisely determined for each orientation of the fragment in space).

In this respect, the generalized model for estimation of an irregularly shaped body trajectory, presented in this research, represents a significant step towards better understanding of flight dynamics of such bodies and can be used in a number of applications.

2. Physical model

Generally, determining the position of the body during the motion through atmosphere includes determining the position of the moving coordinate system (fixed to the rigid body) in relation to the fixed (inertial) reference (coordinate) system.

The orientation of the body in relation to the reference coordinate system is determined by three Euler angles (ψ, θ, ϕ) and three coordinates (x, y, z) that define the position of the body relative to the given system.
Thus, the position of the moving coordinate system in relation to the fixed reference system is determined by six coordinates.

The number of degrees of freedom of movement of the material system is the number of independently variable coordinates that completely determine the position of all points of that system in the space. This means that the free body during the motion through the air has six degrees of freedom, i.e. it can perform six independent movements, three translations along axes of the fixed coordinate system, and three independent rotations defined by the Euler angles.

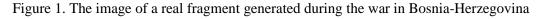The final equations of the motion of the free rigid body have the following form:

$$x = x(t), \quad y = y(t), \quad z = z(t), \tag{1a}$$
$$\psi = \psi(t), \quad \theta = \theta(t), \quad \phi = \phi(t). \tag{1b}$$

The three equations in the expression (1a) determine the translation of the center mass of the body, while the last three equations in the expression (1b) determine the spherical motion around the center of the mass of the body.

During the motion of the body, all six coordinates change as a function of time. In the developed model of an irregularly shaped body (fragment) motion through the atmosphere, the following assumptions are adopted:
- The fragment (Fig.1) is a rigid body (the size and shape of a fragment do not change over time).
- The inertial (fixed) coordinate system is tied to the Earth.
- The exposed (projected) surface of the fragment is determined by the methodology described in the previous related study [14], where the fragment is approximated by a tri-axial ellipsoid.
- The aerodynamic force and the aerodynamic moment acting on the fragment are determined using the model presented in the previous related work [15].

Figure 1. The image of a real fragment generated during the war in Bosnia-Herzegovina

- The moving coordinate system is located in the fragment center of mass (Figures 2 and 3) and its axes coincide with the principal axes of inertia for fragment. Generally, it is always possible to determine the orientation of the coordinate system bound to the body for which the centrifugal moments of the inertia will be zero.

  In this case, three mutual axes are called the principal axes of inertia, and the corresponding moments of inertia are the principal moments of inertia. Since the fragment is not symmetrical (stochastic, irregular shape), the coordinate system rigidly bound to the fragment in its center of mass (Fig. 2) is defined so that it coincides with the principal axes of inertia (the fragment is approximated by tri-axial ellipsoid) for which the centrifugal moments of inertia are zero.

Figure 2 shows the free body diagram of the fragment during its motion through the resistive medium, such as air. The figure shows the vectors of the total aerodynamic force $\vec{F}_{ad}$, aerodynamic moment $\vec{M}_{ad}$, and gravity force $m\vec{g}$. The aerodynamic force is distributed all over the surface of the fragment, but the equivalent place where the total aerodynamic force is acting is the center of pressure (CP). However, more convenient for the further dynamical analysis is to transfer all aerodynamical resistance to the center of gravity (C). In this way, the total aerodynamical force is transferred to the center of gravity, and the corresponding aerodynamical moment is equal $\vec{M}_{ad} = \vec{r}_{CP} \times \vec{F}_{ad}$. This moment is actually calculated directly in the way that elementary force $d\vec{F}_{ad}$ is calculated for every element of the surface of the fragment and right away the elementary moment is calculated as $d\vec{M}_{ad} = \vec{r} \times d\vec{F}_{ad}$.
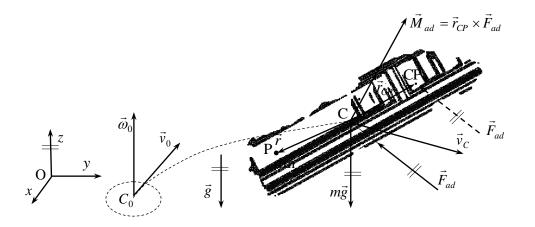

Figure 2. Free body diagram of the fragment and equivalent force and moment acting at the center of gravity

Figure 3 shows the coordinate system tied to the Earth (xyz) and the moving system tied to the fragment ($\xi\eta\zeta$). The angular velocity $\vec{\omega}$ is consisted of the three components $\vec{\omega} = \vec{\omega}_1 + \vec{\omega}_2 + \vec{\omega}_3$. The corresponding three Euler's angles are: ψ (angle of precession), θ (angle of nutation) and φ (angle of intrinsic rotation). These angles determine the spherical movement around the center of the body mass, i.e., defines the orientation of the body relative to the reference coordinate system $x_1y_1z_1$ which travels with the body but stays parallel to the coordinate system xyz tied to the Earth.

The coordinate system $\xi\eta\zeta$ has the three indices, where the first one is obtained after the precession, the second one after the nutation and the third one after the intrinsic spinning about the third axis tight to the body. For the convenience of further calculations, the index of the body attached axes, after the third rotation, is removed, which means $\xi_3 \equiv \xi$, $\eta_3 \equiv \eta$ and $\zeta_3 \equiv \zeta$.
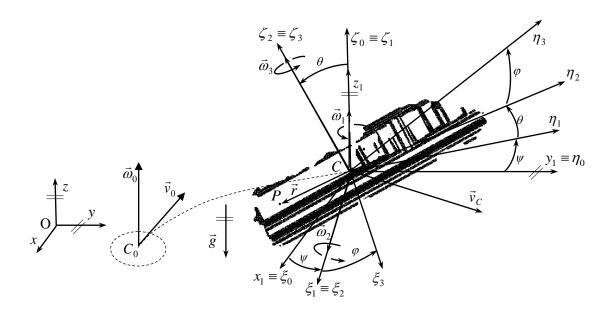
Figure 3. Visualization of coordinate systems and kinematic parameters during the movement of fragment through the resistive medium

Differential equations of the translational motion component in a coordinate system rigidly connected to the body, are set using the law of the body center of mass movement:

$$m\vec{a}_c = m\frac{d\vec{V}}{dt} = \sum_{i=1}^{n}\vec{F}_i \ , \tag{2}$$

where: $\vec{F}_i$ - external forces, m – body mass, $\vec{a}$ and $\vec{V}$ - acceleration and velocity of the body center of mass.

External forces acting on a fragment are an aerodynamic force and a force of gravity, so the expression (2) can be represented as

$$m\vec{a}_c = \vec{F}_{ad} + m\vec{g} \ . \tag{3}$$

Differential equations of rotation around the body center of the mass are obtained using the law of change of angular momentum:

$$\frac{d\vec{L}_c}{dt} = \sum_{i=1}^{n}\vec{M}_i \ . \tag{4}$$

Here $\vec{M}$ is vector of the aerodynamic moment, a $\vec{L}$ - angular momentum vector in moving coordinate system tied to the body.

First, based on the expression (4), the expressions for the angular velocity and Euler angles (that define the orientation of the body in the space in relation to the fixed coordinate system) will be derived, and then the expressions for determining translational velocity and coordinates of the body (trajectories) in the space.

Aerodynamic moment $\vec{M}_{ad}$ acts on a fragment, so expression (4) can be written as:

$$\frac{d\vec{L}_c}{dt} = \vec{M}_{ad} \ . \tag{5}$$

Angular momentum vector $\vec{L}_c$ for mass m on distance $\vec{r}$ from the center of mass, is given by expression:

$$\vec{L}_c = \int_m \left[\vec{r} \times \vec{v} dm \right] \tag{6}$$

In expression (6) $\vec{r}$ is radius vector of an arbitrary point on a body (point P in Fig. 4):

$$\vec{r} = \overrightarrow{CP} = [\xi, \eta, \zeta]_{\xi\eta\zeta} . \tag{7}$$

As can be seen from (7), the vector $\vec{r}$ is given over the coordinate of the moving coordinate system $0\xi\eta\zeta$ (Fig. 4), rigidly bound to the (moving) fragment.

The velocity vector from expression (6) can be represented as a sum of the velocity vector of the center of mass and the velocity vector around the center of mass for a given body:

$$\vec{v} = \vec{v}_c + \vec{v}_p = \vec{v}_c + \left[\vec{\omega} \times \vec{r} \right]. \tag{8}$$

Also, the angular velocity (in two coordinate systems, $0xyz$ and $0\xi\eta\zeta$) can be represented by the expressions:

$$\left| \vec{\omega} \right| = \sqrt{\omega_x^2 + \omega_y^2 + \omega_z^2} = \sqrt{\omega_\xi^2 + \omega_\eta^2 + \omega_\zeta^2} . \tag{9}$$

Using previous expressions, the angular momentum is:

$$\vec{L}_c = \int_m \left[\vec{r} \times \left(\vec{v}_c + \left[\vec{\omega} \times \vec{r} \right] \right) \right] dm = \int_m \left[\vec{r} \times \vec{v}_c \right] dm + \int_m \left[\vec{r} \times \left[\vec{\omega} \times \vec{r} \right] \right] dm . \tag{10}$$

Figure 4 presents kinematic parameters that appear in the model and it shows a fixed coordinate system tied to Earth ($0xyz$), as well as the moving coordinate $0\xi\eta\zeta$ rigidly tied to the body. Euler angles ψ, θ and φ, as well as the components of angular velocity vector are also presented. The current rotating axis of the body is represented in Fig. 4 as Ω-Ω. Angular momentum vector $\vec{L}_c$ is also shown in the figure.
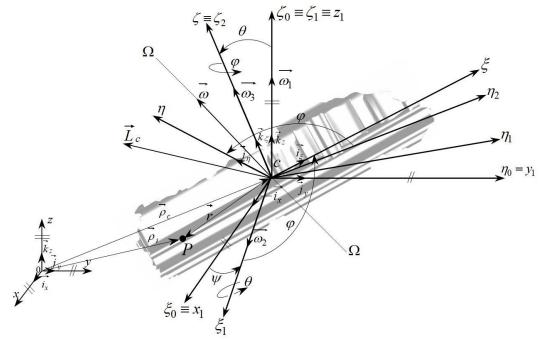

Figure 4. Kinematic parameters in the model

The first part on the right side of the expression (10) is equal to zero:

$$\int_m \left[\vec{r} \times \vec{v}_c\right] dm = \sum_i \left(\left(\vec{\rho}_i - \vec{\rho}_c\right) \times \vec{v}_c\right) m_i = \sum_i \left(\vec{\rho}_i \times \vec{v}_c\right) m_i - \sum_i \left(\vec{\rho}_c \times \vec{v}_c\right) m_i = 0 \text{ , because} \tag{11}$$

by cross product of the $\sum_i m_i \vec{\rho}_i = m\vec{\rho}_C$, (by the definition of the cg position) with the vector $\vec{v}_C$ from the right hand side, which is independent on the point position (constant for the considered instant), the following is obtained:

$$\sum_i \left(\vec{\rho}_i m_i\right) \times \vec{v}_c = \sum_i \left(\vec{\rho}_i \times \vec{v}_c\right) m_i = \sum_i \left(\left(\vec{\rho}_i m_i\right) \times \vec{v}_c\right) = \sum_i \left(\vec{\rho}_i m_i\right) \times \vec{v}_c = m\vec{\rho}_c \times \vec{v}_c \text{ ,} \tag{12}$$

where $\vec{\rho}_i, \vec{\rho}_c$ are vectors of the point P and the body center of mass C (Fig. 4) respectively, relative to the fixed coordinate system $0xyz$ attached to the ground.

For the moving coordinate system $C\xi\eta\zeta$ (Fig. 3) the rotational velocity of an arbitrary point at the body surface:

$$\left[\vec{\omega} \times \vec{r}\right] = \begin{vmatrix} \vec{i} & \vec{j} & \vec{k} \\ \omega_\xi & \omega_\eta & \omega_\zeta \\ \xi & \eta & \zeta \end{vmatrix} = \left(\zeta\omega_\eta - \eta\omega_\zeta\right)\vec{i} + \left(\xi\omega_\zeta - \zeta\omega_\xi\right)\vec{j} + \left(\eta\omega_\xi - \xi\omega_\eta\right)\vec{k} \text{ ,} \tag{13}$$

such that the moment of the velocity vector for the center of gravity is:

$$\left[\vec{r} \times \left[\vec{\omega} \times \vec{r}\right]\right] = \begin{vmatrix} \vec{i} & \vec{j} & \vec{k} \\ \xi & \eta & \zeta \\ \zeta\omega_\eta - \eta\omega_\zeta & \xi\omega_\zeta - \zeta\omega_\xi & \eta\omega_\xi - \xi\omega_\eta \end{vmatrix}. \tag{14}$$

The term (14) in the developed form is:

$$\left[\vec{r} \times \left[\vec{\omega} \times \vec{r}\right]\right] = \left(\eta^2\omega_\xi - \eta\xi\omega_\eta - \xi\zeta\omega_\zeta + \zeta^2\omega_\xi\right)\vec{i}_\xi + \left(\zeta^2\omega_\eta - \zeta\eta\omega_\zeta - \xi\eta\omega_\xi + \xi^2\omega_\eta\right)\vec{j}_\eta + \left(\xi^2\omega_\zeta - \xi\zeta\omega_\xi - \zeta\eta\omega_\eta + \eta^2\omega_\zeta\right)\vec{k}_\zeta. \tag{15}$$

It can be written (based on 11 and 15):

$$\vec{L}_c = \left(I_\xi\omega_\xi - I_{\xi\eta}\omega_\eta - I_{\xi\zeta}\omega_\zeta\right)\vec{i}_\xi + \left(-I_{\xi\eta}\omega_\xi + I_\eta\omega_\eta - I_{\eta\zeta}\omega_\zeta\right)\vec{j}_\eta + \left(-I_{\xi\zeta}\omega_\xi - I_{\eta\zeta}\omega_\eta + I_\zeta\omega_\zeta\right)\vec{k}_\zeta \text{ ,} \tag{16}$$

or in a matrix form, using the inertia tensor I:

$$\vec{L}_c = \begin{bmatrix} I_{\xi\xi} & -I_{\xi\eta} & -I_{\xi\zeta} \\ -I_{\xi\eta} & I_{\eta\eta} & -I_{\eta\zeta} \\ -I_{\xi\zeta} & -I_{\eta\zeta} & I_{\zeta\zeta} \end{bmatrix} \begin{bmatrix} \omega_\xi \\ \omega_\eta \\ \omega_\zeta \end{bmatrix}. \tag{17}$$

In the expression (17) $I_{\xi\xi}$, $I_{\eta\eta}$ and $I_{\zeta\zeta}$ are moments of inertia for axes ζ, η and ζ (Fig. 3 and Fig. 4) in the coordinate system rigidly bound to the body, and $I_{\xi\eta}$, $I_{\eta\zeta}$ and $I_{\xi\zeta}$ are the products of inertia. Based on the expression (16):

$$\frac{d\vec{L}_c}{dt} = \left(I_\xi \dot{\omega}_\xi - I_{\xi\eta}\dot{\omega}_\eta - I_{\xi\zeta}\dot{\omega}_\zeta\right)\vec{i}_\xi + \left(I_\xi \omega_\xi - I_{\xi\eta}\omega_\eta - I_{\xi\zeta}\omega_\zeta\right)\frac{d\vec{i}_\xi}{dt}$$
$$+ \left(-I_{\xi\eta}\dot{\omega}_\xi + I_\eta \dot{\omega}_\eta - I_{\eta\zeta}\dot{\omega}_\zeta\right)\vec{j}_\eta + \left(-I_{\xi\eta}\omega_\xi + I_\eta \omega_\eta - I_{\eta\zeta}\omega_\zeta\right)\frac{d\vec{j}_\eta}{dt} \tag{18}$$
$$+ \left(-I_{\xi\zeta}\dot{\omega}_\xi - I_{\eta\zeta}\dot{\omega}_\eta + I_\zeta \dot{\omega}_\zeta\right)\vec{k}_\zeta + \left(-I_{\xi\zeta}\omega_\xi - I_{\eta\zeta}\omega_\eta + I_\zeta \omega_\zeta\right)\frac{d\vec{k}_\zeta}{dt}.$$

where:

$$\frac{d\vec{i}_\xi}{dt} = \left[\vec{\omega} \times \vec{i}_\xi\right], \tag{19a}$$

$$\frac{d\vec{j}_\eta}{dt} = \left[\vec{\omega} \times \vec{j}_\eta\right], \tag{19b}$$

$$\frac{d\vec{k}_\zeta}{dt} = \left[\vec{\omega} \times \vec{k}_\zeta\right]. \tag{19c}$$

The expression (16) can also be written in the following form:

$$\vec{L}_c = \vec{L}_{c\xi}\vec{i}_\xi + \vec{L}_{c\eta}\vec{j}_\eta + \vec{L}_{c\zeta}\vec{k}_\zeta \tag{20}$$

and it follows (after the derivation of angular momentum vector $\vec{L}_c$):

$$\frac{d\vec{L}_c}{dt} = \dot{L}_{c\xi}\vec{i}_\xi + L_{c\xi}\frac{d\vec{i}_\xi}{dt} + \dot{L}_{c\eta}\vec{j}_\eta + L_{c\eta}\frac{d\vec{j}_\eta}{dt} + \dot{L}_{c\zeta}\vec{k}_\zeta + L_{c\zeta}\frac{d\vec{k}_\zeta}{dt}. \tag{21}$$

The term (21) can be written somewhat differently if several members are grouped in the following form:

$$\frac{d\vec{L}_c}{dt} = \dot{L}_{c\xi}\vec{i}_\xi + \dot{L}_{c\eta}\vec{j}_\eta + \dot{L}_{c\zeta}\vec{k}_\zeta + L_{c\xi}\frac{d\vec{i}_\xi}{dt} + L_{c\eta}\frac{d\vec{j}_\eta}{dt} + L_{c\zeta}\frac{d\vec{k}_\zeta}{dt}. \tag{22}$$

This expression can be written in a general form whereby individual members can be more easily identified and how they affect the change in angular momentum:

$$\left.\frac{d\vec{L}_c}{dt}\right|_{fixed\_coord\_sys.}^{total\_change} = \left.\frac{\delta\vec{L}_c}{\delta t}\right|_{moving-coord\_sys.}^{loc.\,change} + \left[\vec{\omega} \times \vec{L}_c\right]^{change\,of\,\vec{L}_c\,due\,to\,rotation\,of\,the\,coord.\,frame}. \tag{23}$$

The expression on the left side of (23) represents the change in the angular momentum "seen" from the fixed coordinate system $0xyz$, and the first expression on the right of (23) represents the change of angular momentum "seen" from the moving coordinate system $0\xi\eta\zeta$. The second expression on the right side of (23) is a consequence of a rotation of the coordinate frame that is used to express the angular momentum.

Using expressions (5), and expressions (18) - (23) on symmetric bodies (for which the products of inertia are equal to zero), following expressions are valid (for the coordinate system $0\xi\eta\zeta$ tied to the body):

$$I_\xi \dot{\omega}_\xi + \left[\vec{\omega} \times \vec{L}_c\right]_\xi = M_{ad\,\xi}, \tag{24a}$$

$$I_\eta \dot{\omega}_\eta + \left[\vec{\omega} \times \vec{L}_c\right]_\eta = M_{ad\,\eta} \text{,} \tag{24b}$$

$$I_\zeta \dot{\omega}_\zeta + \left[\vec{\omega} \times \vec{L}_c\right]_\zeta = M_{ad\,\zeta} \text{.} \tag{24c}$$

Since:

$$\left[\vec{\omega} \times \vec{L}_c\right]_\xi = \omega_\eta \omega_\zeta \left(I_\zeta - I_\eta\right), \tag{25a}$$

$$\left[\vec{\omega} \times \vec{L}_c\right]_\eta = \omega_\xi \omega_\zeta \left(I_\xi - I_\zeta\right), \tag{25b}$$

$$\left[\vec{\omega} \times \vec{L}_c\right]_\zeta = \omega_\xi \omega_\eta \left(I_\eta - I_\xi\right). \tag{25c}$$

From (24 and 25) follows:

$$\dot{\omega}_\xi = \frac{1}{I_\xi}\left[M_{ad\,\xi} - \omega_\eta \omega_\zeta \left(I_\zeta - I_\eta\right)\right], \tag{26a}$$

$$\dot{\omega}_\eta = \frac{1}{I_\eta}\left[M_{ad\,\eta} - \omega_\xi \omega_\zeta \left(I_\xi - I_\zeta\right)\right], \tag{26b}$$

$$\dot{\omega}_\zeta = \frac{1}{I_\zeta}\left[M_{ad\,\zeta} - \omega_\xi \omega_\eta \left(I_\eta - I_\xi\right)\right]. \tag{26c}$$

Moments of inertia that appear in the expression (26) for the ellipsoid (which approximates irregularly shaped fragment in the model) which is assumed to have a uniform density are determined by the following expressions:

$$I_\xi = I_{\xi\xi} = \frac{m}{5}\left(b^2 + c^2\right), \quad I_\eta = I_{\eta\eta} = \frac{m}{5}\left(a^2 + c^2\right), \quad I_\zeta = I_{\zeta\zeta} = \frac{m}{5}\left(a^2 + b^2\right) \tag{27}$$

Here a, b, and c are the half-axes of a tri-axial ellipsoid that represents the fragment (as described in the previous related papers [14, 15]). When axes ξ, η, ζ of the moving coordinate system $0\xi\eta\zeta$, rigidly bound to the fragment, at the same time are principal axes of inertia, then the products if inertia is zero, and the following can be written:

$$I_{\xi\eta} = I_{\eta\zeta} = I_{\xi\zeta} = 0 \text{.} \tag{28}$$

Generally speaking, the first rotation of the body $\vec{\omega}_1$ is precession around the fixed axis (Fig. 4). The nutation is with angular velocity $\vec{\omega}_2$ around the moving axis and the third rotation is intrinsic rotation about moving axis with angular velocity $\vec{\omega}_3$. Three rotations can be replaced with one (total) angular velocity $\vec{\omega}$:

$$\vec{\omega} = \vec{\omega}_1 + \vec{\omega}_2 + \vec{\omega}_3 \text{.} \tag{29}$$

Here the direction of the total angular velocity vector defines the direction of the current rotation axis (designated as Ω-Ω in Fig. 4).

The components in (29) are defined as Euler's angles:

$$\omega_1 = \dot{\psi}, \quad \omega_2 = \dot{\theta}, \quad \omega_3 = \dot{\varphi} \text{.} \tag{30}$$

From (29) and (30) it can be written:

$$\vec{\omega} = \dot{\psi}\vec{k}_z + \dot{\theta}\vec{i}_\xi + \dot{\varphi}\vec{k}_\zeta . \tag{31}$$

The angular velocity projections (via Euler angles) on axes of the moving coordinate system $0\xi\eta\zeta$ are defined with expressions:

$$\omega_\xi = \omega_1 \sin\theta \sin\varphi + \omega_2 \cos\varphi = \dot{\psi}\sin\theta \sin\varphi + \dot{\theta}\cos\varphi , \tag{32a}$$

$$\omega_\eta = \omega_1 \sin\theta \cos\varphi - \omega_2 \sin\varphi = \dot{\psi}\sin\theta \cos\varphi - \dot{\theta}\sin\varphi , \tag{32b}$$

$$\omega_\zeta = \omega_1 \cos\theta + \omega_3 = \dot{\psi}\cos\theta + \dot{\varphi}. \tag{32c}$$

From the expression (32), the Euler angles ψ, θ and φ can be determined by substitution:

$$\dot{\psi} = \left(\frac{1}{\sin\theta}\right)(\omega_\xi \sin\varphi + \omega_\eta \cos\varphi), \tag{33a}$$

$$\dot{\theta} = \left(\frac{1}{\cos\varphi}\right)(\omega_\xi - \dot{\psi}\sin\theta \sin\varphi), \tag{33b}$$

$$\dot{\varphi} = \omega_\zeta - \dot{\psi}\cos\theta . \tag{33c}$$

By differentiating the expression (32) we obtain:

$$\dot{\omega}_\xi = \ddot{\psi}\sin\theta \sin\varphi + \dot{\psi}\dot{\theta}\cos\theta \sin\varphi + \dot{\psi}\dot{\varphi}\sin\theta \cos\varphi + \ddot{\theta}\cos\varphi - \dot{\theta}\dot{\varphi}\sin\varphi , \tag{34a}$$

$$\dot{\omega}_\eta = \ddot{\psi}\sin\theta \cos\varphi + \dot{\psi}\dot{\theta}\cos\theta \cos\varphi - \dot{\psi}\dot{\varphi}\sin\theta \sin\varphi - \ddot{\theta}\sin\varphi - \dot{\theta}\dot{\varphi}\cos\varphi , \tag{34b}$$

$$\dot{\omega}_\zeta = \ddot{\psi}\cos\theta - \dot{\psi}\dot{\theta}\sin\theta + \ddot{\varphi}. \tag{34c}$$

Expressions from (34) can be written in abbreviated form:

$$\ddot{\psi}\sin\theta \sin\varphi + \ddot{\theta}\cos\varphi = a_1 + b_1 = d_1 , \tag{35a}$$

$$\ddot{\psi}\sin\theta \cos\varphi - \ddot{\theta}\sin\varphi = a_2 + b_2 = d_2 , \tag{35b}$$

$$\ddot{\psi}\cos\theta + \ddot{\varphi} = a_3 + b_3 = d_3 , \tag{35c}$$

where:

$$a_1 = \dot{\omega}_\xi , \tag{36a}$$

$$a_2 = \dot{\omega}_\eta , \tag{36b}$$

$$a_3 = \dot{\omega}_\zeta , \tag{36c}$$

$$b_1 = \dot{\theta}\dot{\varphi}\sin\varphi - \dot{\psi}\dot{\theta}\cos\theta \sin\varphi - \dot{\psi}\dot{\varphi}\sin\theta \cos\varphi , \tag{36d}$$

$$b_2 = \dot{\theta}\dot{\varphi}\cos\varphi - \dot{\psi}\dot{\theta}\cos\theta \cos\varphi + \dot{\psi}\dot{\varphi}\sin\theta \sin\varphi , \tag{36e}$$

$$b_3 = \dot{\psi}\dot{\theta}\sin\theta . \tag{36f}$$

If the expression (35a) is multiplied by $\sin\varphi$, and (35b) with $\cos\varphi$, and if the two new terms are added together:

$$\ddot{\psi}\left(\sin\theta \sin^2\varphi + \sin\theta \cos^2\varphi\right) = d_1 \sin\varphi + d_2 \cos\varphi . \tag{37}$$

From this, the double derivative of the angle ψ is:

$$\ddot{\psi} = \frac{1}{\sin\theta}\left(d_1 \sin\varphi + d_2 \cos\varphi\right), \qquad (38)$$

From (35b) the nutation angle is:

$$\ddot{\theta} = \frac{1}{(\cos\varphi)}\left(d_1 - \ddot{\psi}\sin\theta\sin\varphi\right). \qquad (39)$$

From (35c) angle of the intrinsic rotation:

$$\ddot{\varphi} = d3 - \ddot{\psi}\cos\theta. \qquad (40)$$

The following is the derivation of the law of the body center of mass movement. By projecting, previously given equations (3), on axes of the inertial (fixed) coordinate system $Oxyz$ (Figures 3 and 4), the following expressions are obtained:

$$m\ddot{x}_c = F_{ad_x}, \qquad (41a)$$

$$m\ddot{y}_c = F_{ad_y}, \qquad (41b)$$

$$m\ddot{z}_c = F_{ad_z} - mg. \qquad (41c)$$

In order to obtain the value of the force $\vec{F}_{ad}$, projected on the coordinate system $Oxyz$, the transformation matrix R is used, which is obtained by multiplication of individual matrices that define the rotation of the body around certain axes:

$$R = R_\psi R_\theta R_\varphi = \begin{bmatrix} \cos\psi & -\sin\psi & 0 \\ \sin\psi & \cos\psi & 0 \\ 0 & 0 & 1 \end{bmatrix}\begin{bmatrix} 1 & 0 & 0 \\ 0 & \cos\theta & -\sin\theta \\ 0 & \sin\theta & \cos\theta \end{bmatrix}\begin{bmatrix} \cos\varphi & -\sin\varphi & 0 \\ \sin\varphi & \cos\varphi & 0 \\ 0 & 0 & 1 \end{bmatrix}. \qquad (42)$$

The multiplication of the first two matrices results in:

$$R = R_\psi R_\theta R_\varphi = \begin{bmatrix} \cos\psi & -\sin\psi\cos\theta & \sin\psi\sin\theta \\ \sin\psi & \cos\psi\cos\theta & -\cos\psi\sin\theta \\ 0 & \sin\theta & \cos\theta \end{bmatrix}\begin{bmatrix} \cos\varphi & -\sin\varphi & 0 \\ \sin\varphi & \cos\varphi & 0 \\ 0 & 0 & 1 \end{bmatrix}. \qquad (43)$$

Finally, the transformation matrix R is:

$$R = \begin{bmatrix} \cos\psi\cos\varphi - \sin\psi\cos\theta\sin\varphi & -\cos\psi\sin\varphi - \sin\psi\cos\theta\cos\varphi & \sin\psi\sin\theta \\ \sin\psi\cos\varphi + \cos\psi\cos\theta\sin\varphi & -\sin\psi\sin\varphi + \cos\psi\cos\theta\cos\varphi & -\cos\psi\sin\theta \\ \sin\theta\sin\varphi & \sin\theta\cos\varphi & \cos\theta \end{bmatrix}. \qquad (44)$$

So it can be written for the aerodynamic force:

$$\begin{bmatrix} F_{ad_x} \\ F_{ad_y} \\ F_{ad_z} \end{bmatrix} = R\begin{bmatrix} F_{ad_\xi} \\ F_{ad_\eta} \\ F_{ad_\zeta} \end{bmatrix}. \qquad (45)$$

Using expressions (44) and (45) the following is obtained:

$$\begin{bmatrix} F_{ad_x} \\ F_{ad_y} \\ F_{ad_z} \end{bmatrix} = \begin{bmatrix} (\cos\psi\cos\varphi - \sin\psi\cos\theta\sin\varphi)F_{ad_\xi} & (-\cos\psi\sin\varphi - \sin\psi\cos\theta\cos\varphi)F_{ad_\eta} & (\sin\psi\sin\theta)F_{ad_\zeta} \\ (\sin\psi\cos\varphi + \cos\psi\cos\theta\sin\varphi)F_{ad_\xi} & (-\sin\psi\sin\varphi + \cos\psi\cos\theta\cos\varphi)F_{ad_\eta} & (-\cos\psi\sin\theta)F_{ad_\zeta} \\ (\sin\theta\sin\varphi)F_{ad_\xi} & (\sin\theta\cos\varphi)F_{ad_\eta} & (\cos\theta)F_{ad_\zeta} \end{bmatrix}. \quad (46)$$

Similarly, the following can be written for the aerodynamic moment:

$$\begin{bmatrix} M_{ad_x} \\ M_{ad_y} \\ M_{ad_z} \end{bmatrix} = \begin{bmatrix} (\cos\psi\cos\varphi - \sin\psi\cos\theta\sin\varphi)M_{ad_\xi} & (-\cos\psi\sin\varphi - \sin\psi\cos\theta\cos\varphi)M_{ad_\eta} & (\sin\psi\sin\theta)M_{ad_\zeta} \\ (\sin\psi\cos\varphi + \cos\psi\cos\theta\sin\varphi)M_{ad_\xi} & (-\sin\psi\sin\varphi + \cos\psi\cos\theta\cos\varphi)M_{ad_\eta} & (-\cos\psi\sin\theta)M_{ad_\zeta} \\ (\sin\theta\sin\varphi)M_{ad_\xi} & (\sin\theta\cos\varphi)M_{ad_\eta} & (\cos\theta)M_{ad_\zeta} \end{bmatrix}. \quad (47)$$

3.   MatLab program for calculation of fragment trajectory elements

Generalized (6DOF) model for estimation of an irregularly shaped body trajectory, derived here, is implemented in a computer program, written in MatLab.

Program allows the estimation of essential parameters of the fragment dynamics: trajectory, the translational and the angular velocity, and the estimation of the fragment orientation during the motion. The program contains additional subroutines that serve to calculate the aerodynamic force, moment, and exposed (projected) surface of the fragment. Also, the program uses ode45 solver for integration of a system of differential equations, derived in previous sections. At the end of calculation, the program prints the results and represents them graphically, and also makes on output file (MS Excel document) with results (time, coordinates of the center of mass, translational velocity components, Euler angles and angular velocity components).

The initial conditions of the program, written in MatLab, are:
   − *Mass parameters of the fragment*. Moments of inertia are determined using expressions in (27). In order to determine the mass and moments of inertia (fragment approximated by a tri-axial ellipsoid), as input parameters only the values of the ellipsoid half-axes *a*, *b* and *c* are needed.
   The formula for the volume of an ellipsoid is:

$$V_{elipsoid} = \frac{4}{3}abc\pi, \qquad (48)$$

where *a*, *b* i *c* are ellipsoid half-axes. Mass of an ellipsoid is then:

$$m_{elipsoid} = \frac{4}{3}\rho abc\pi, \qquad (49)$$

where ρ is density of fragment material (steel). When the mass and fragment dimensions are known, moments of inertia are determined using expression (27).

   − *The initial position of the body*. Coordinates of the fragment relative to the fixed coordinate system *0xyz* (Fig. 3). For real HE fragment fragments, these coordinates correspond to the coordinates of the centers of the different segments of the projectile body (relative to the coordinate system tied to the ground - usually defined at the top of the projectile fuze).
   − *The initial orientation of the body*. Initial angles relative to the coordinate system *0xyz*. Figure 5 shows the initial (zero) position of the body in the calculation of irregularly body trajectories in accordance with the physical model. The initial zero position (or reference position) is a special case of the initial position at which the angles are zero. Generally, the initial position is an arbitrary position, with arbitrary angles according to the initial orientation of the fragment. In the model and program, the gravity force is directed in the negative direction of axis *z* (Fig. 4).
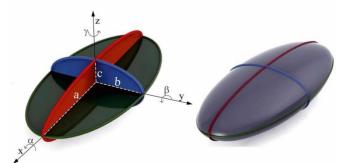
Figure 5. Initial zero position of the ellipsoidal body in the Matlab program for the calculation of irregularly shaped body trajectory

For the sake of visualization, the orientation of the fragment in the program is defined by absolute angles (α, β, γ; Fig. 5) around the coordinate axes of the translational coordinate system tied to the inertia center. The link between these angles with the Euler angles is given by the total rotation matrix R_t around the translational coordinate system:

$$R_t = R_\gamma R_\beta R_\alpha = \begin{bmatrix} \cos\gamma & -\sin\gamma & 0 \\ \sin\gamma & \cos\gamma & 0 \\ 0 & 0 & 1 \end{bmatrix} \begin{bmatrix} \cos\beta & 0 & \sin\beta \\ 0 & 1 & 0 \\ -\sin\beta & 0 & \cos\beta \end{bmatrix} \begin{bmatrix} 1 & 0 & 0 \\ 0 & \cos\alpha & -\sin\alpha \\ 0 & \sin\alpha & \cos\alpha \end{bmatrix} \quad (50)$$

Here α is rotation around axis x, β around axis y, and γ around axis z. The total rotation matrix over the angles (ψ, θ, φ) of the moving coordinate system previously defined, rigidly bound to the body, and the total rotation matrix over the absolute angles (α, β, γ) around the translational coordinate system bound to the center of inertia, is equal, i.e. it gives the same orientation of the body - which gives a closed equation system (R = Rt).

− *The initial velocity of fragments.* The value of the initial translational velocity of fragments is determined by the Gurney method (as explained in an earlier paper [16]), depending on the segment of the projectile (ratio of explosive to body mass) and explosive charge type and density.

− *Initial angular velocity of fragments.* The values of the initial angular velocity of fragments must be assumed because their values can vary greatly and can have any value. Namely, it is difficult to find usable data on the value of the initial angular velocity of fragments. According to some researches, the initial angular velocity of fragments does not exceed the value of 50 rot/s [13], and some mention values of up to 3650 rot/s [12]. Since researches from reference [13] were more oriented to experimental tests (and researches from reference [12] were oriented to numerical simulations), the maximum value of 50 rot/s is closer to the real case.

Program for modeling a fragment dynamics solves for the trajectory of a fragment using a model for calculation of aerodynamic force and moment. The translational part is solved by predicting the aerodynamic force and using it in the dynamic equations of motion. The rotational part is solved by predicting the aerodynamic moment. During the calculation, the program calls a function that gives the derivatives for the differential equations of motion for the fragment. The function provides the current derivatives values of the system of differential equations of a rigid body (fragment) motion through a resistive medium. It calls another function which uses a model [15] in order to provide the external force and moment in a vector form. The full set of equations of motion is solved (6 differential equations of second order, which are represented as an expanded set of equations of the first order). Inputs in this function are the set of variables representing the dynamic state and current time value, all provided by the calling function in the main program.

Outputs in this function are the vector (12x1) of the current derivatives of the vector representing the current dynamic state of the rigid body motion. This function calls another function for estimation of aerodynamic force and aerodynamic moment for a given orientation of a rigid body.

The output data from the main program are written into special MS Excel file that can be later processed and analyzed.

Output data are:
  – the flight time of the fragment,
  – coordinates of fragment mass center,
  – translation velocity components,
  – angular velocity components,
  – Fragment orientation during flight.

The program output data can be printed in a different format, which can be defined within the program itself. Also, the program allows for interactive chart drawing (trajectory, velocity change, etc.).

The described model for estimation of fragment trajectory, and the Matlab program calculating the required parameters have several advantages.

First of all, the program is parametric and can interactively change individual parameters (fragment dimensions, initial conditions). Furthermore, the program finishes the calculation (depending on the number of time steps and initial conditions as well as the computer's characteristics) much faster than it would be the case using 6DOF in CFD programs (i.e. in Ansys Fluent). Specifically, 6DOF simulation of irregular shape bodies in CFD programs (i.e. [11]) requires high performance (large number of processors) and appropriate software.

An additional advantage of the model is that it does not require a database of aerodynamic coefficients (which are otherwise problematic due to irregular and stochastic geometry of fragments) because it contains a separate model for estimating aerodynamic force and moment [15] based on the shape of the fragment and the initial velocity vector. Also, this model estimates the real value of the projected (exposed) surface of the body (a fragment approximated by the ellipsoid), perpendicular to the velocity vector, unlike other models where the exposed surface is taken either as a constant or determined by statistical methods.

4. Analysis of results

The calculation of the complete trajectory of the irregularly shaped fragments can be used in the analysis of the effects of the fragments - i.e. the safety analysis of the location of the ammunition storages/depots (due to the potential explosion of the projectile) or ie. the danger of demining larger quantities of the munition. In other words, this calculation can be used whenever it is necessary to estimate the maximum range of fragments around locations where explosives and munition are located.

The calculation of the trajectories for such a fragment at various initial elevation angles was performed for a fragment with a mass of 7.89g (the dimensions of the semi-axes of the approximate tri-axial ellipsoid were: a = 10mm, b = 6mm and c = 4mm). The (initial) elevation angle is defined by the angles of the velocity vector (and its intensity) relative to the coordinate ores. It is set that $\beta_v=90°$ (angle between the velocity vector and axis y; Fig. 5), so the elevation angle in this analysis is defined as the angle between the velocity vector and the coordinate axis x.

The total initial velocity in each individual case in this analysis was the same and amounted to 1000 m/s (this corresponds approximately to average initial velocity of fragments from central segment of our artill. projectile 130mm HE M79).

The initial height of the fragment, in this case, was $z_0 = 0.2$m, simulating the position of the fragment on a particular segment of the detonating projectile body in possible real case scenario.

The initial orientation of the fragment, i.e. the absolute angles α_0, β_0 and γ_0, were 45° in this analysis. Angle values are given arbitrarily because they can have any value at the beginning of the movement. Regarding the

initial angular velocity values for each elevation angle, it is assumed that in this analysis, each component of the angular velocity is 50 rev/s (314.16 rad/s), similar to the order of magnitude as the initial angular of velocity referred to in the available experimental studies [13].

Gravitation acceleration for our (Sarajevo) latitude (43.8°N) and altitude (518m) is 9.80352 m/s². The calculation of the trajectory for the following initial elevation angles 5°, 10°, 15°, 20°, 30°, 40°, 50°, 60°, 70° and 80° was performed.

Figure 6 provides 3D trajectories (plotted in the MatLab) of the fragment (7.89g mass) for the different initial angles of elevation at defined initial conditions. Plot can be modified in MatLab, but also in other graphics program (addition of titles, etc.).

Figure 6. 3D trajectories, plotted in the MatLab, of the fragment (with 7.89g mass) for the different initial elevation angles

In order to make these 3D trajectories (of the center of the mass of fragments) clearer, in Fig. 7 trajectories are presented in the plane x-z for the same fragment.

The longest range for this fragment (7.89g) was obtained at initial elevation angle of 15 ° and it was around 435m (similar results were obtained by other authors [8]). In order to show lateral (side) movement for this particular fragment, in Fig. 7, the horizontal drift of the fragment in the x-y plane (see also Fig.8) is shown. The largest lateral drift was 41.6m for initial elevation angle of 80°.

The largest drift occurs at higher elevation angles because, for the same conditions, in this case the fragment moves the longest time so consequently has the time to move more in the horizontal plane (lateral force acts longer on the body). In this case, drift is caused by a certain asymmetry of the initial orientation of the fragment (angles α_0, β_0 and γ_0 all have a value of 45°) relative to the velocity vector direction at the initial moment.
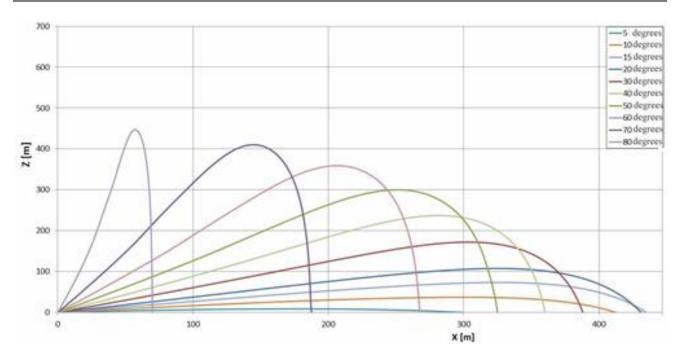
Figure 7. Trajectories of the fragment (7.89g) in the plane x-z
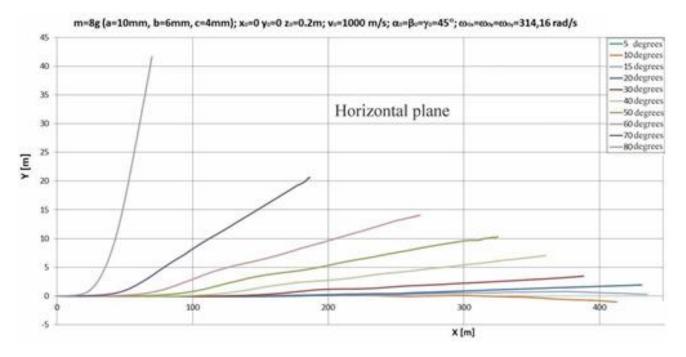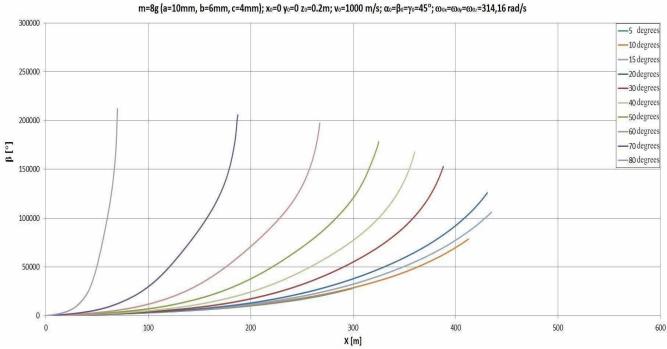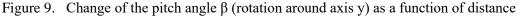

Figure 8. Lateral (side) movement (in the x-y plane) of the fragment with mass 7.89g for different elevation angles
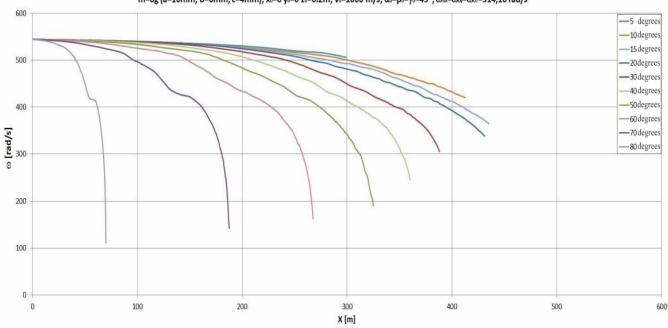
In order to estimate the orientation of fragment (and the number of revolutions) during flight, Fig. 9 shows the change of the pitch angle β (rotation around axis y, shown in Fig. 5) as a function of distance. The change in roll angle α and yaw angle γ is similar to the change of angle β (the initial values of these angles were the same): Because of that, angles (α and γ) were not presented in the additional diagrams. Observing the values of the pitch angle β (Fig. 9), one can observe that a fragment with a mass of 7.89g, at an elevation angle of 80°, during the flight makes 588 full revolutions (around axis y), and at elevation angle of 5° this fragment makes 77 full revolutions (about axis y) until it hits the ground.

Generally, it can be said that in this case fragment will have angular velocity during the whole flight since the flight time is relatively short to make the fragment take a stable orientation during its flight through the atmosphere.

Figure 10 shows changes in the intensity of angular velocity for a given fragment. Since the initial angular velocity components were 314.16 rad/s (50 rev/s), the initial velocity intensity was 544.14 rad/s. During the time of flight, the intensity of the angular velocity decreases. Because for larger elevation angles the fragment flies longer, for these cases the intensity of the angular velocity of the fragments decreases more. So for a fragment with a mass of 7.89g at an elevation angle of 80 °, the intensity of the angular velocity decreased to about 110 rad/s.

Figure 9.   Change of the pitch angle β (rotation around axis y) as a function of distance

Figure 10. Changes in the intensity of angular velocity for the different elevation angles
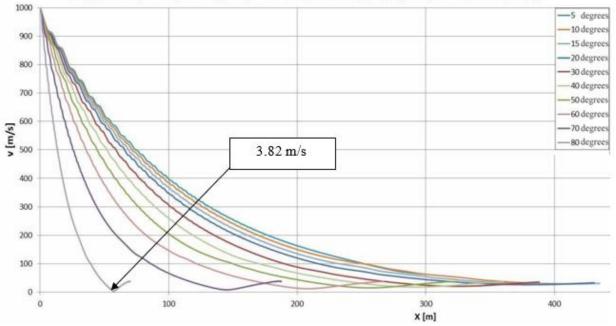
In this analysis, the fragment had an initial angular velocity. If this would be an idealized case where the initial angular velocities would be equal to zero (which does not happen in the real case) then the fragment would have a greater range. In the real situation, however, the fragments always have an initial angular velocity, and during its movement through the air the fragment passes continuously through different orientations with larger or smaller exposed surfaces, and its range is also smaller than would be in an idealized case when there is no initial angular velocity (especially if it would be at an initial orientation with the minimal exposed area of fragment).

It can be noticed that the curves of angular velocity (see Fig. 10) are not continually decreasing but the local value of the angular velocity decreases somewhat faster or slower. This can be explained by the fact that local gradients of angular velocity depend on the current orientation of the fragment so that for certain orientations the aerodynamic moment can have relatively large projections in the negative direction of the angular velocity. This means that for these orientations negative projection of the angular acceleration to the current axis of rotation is relatively high.
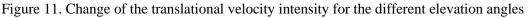
Similar applies also to the translational velocity of the fragments. In Fig. 11 changes in the intensity of the translational velocity for different elevation angles were given. Here also it is noticed that the curves are not continually decreasing but there are different gradients of velocity that cause "wavy" drop of velocity. This also is an effect that results from the continuous rotation of the fragment during its movement. For the 7.89g fragment and for given elevation angles, the rate of velocity decrease is from the initial value of 1000 m/s to about 60 m/s when fragment hits the ground.

Interestingly, the curves of translational velocity in the function of distance (Fig. 11) at higher elevation angles reach their minimum at a certain point, and after that, the velocity of the fragments is slightly increased due to the action of the gravitational force. This happens on the downhill part of the trajectory where the body velocity has been significantly reduced so the velocity is further increased because of the gravity (until the velocity is not equal to the terminal velocity for a given body). Generally speaking, the body achieves terminal velocity when the gravitational force equals the aerodynamic force. Then the total force acting on the body equals zero, so the acceleration is equal to zero, so the velocity becomes constant.

This effect is also present in HE artillery projectiles when fired under large elevation angles. But in the case when the projectile trajectory slope is relatively small, as is the case with anti-armour and small caliber projectiles, with initial velocities usually very large, the velocity does not reach its minimum before the impact point and it is constantly decreasing.

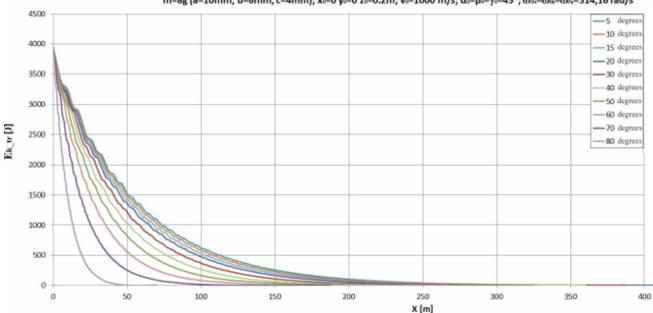Figure 11. Change of the translational velocity intensity for the different elevation angles

The trajectory with the initial elevation angle of about 80 degrees shows rapid velocity decrease and it shows that the magnitude reaches almost zero value. However, it is not actually zero velocity, but a relatively small horizontal velocity, which is negligible with respect to the initial velocity, which caused that this velocity magnitude looks like zero, when displayed at the same diagram along with the initial velocity. Since there is a large deceleration due to the large aerodynamic forces, the velocity magnitude rapidly decreases from the large initial value to the value that is two to three orders smaller than the initial value, such that it is not clearly visible in the same diagram. At the highest level, the vertical component of the velocity is equal to zero. By the time when the fragment reaches the peek position, the horizontal component is much less than the initial horizontal velocity $v_0 cos\phi$ (where ϕ is the elevation angle). Although it looks like there is no velocity at all on the same diagram, there exists relatively small horizontal component at that point, such that the fragment continues traveling when looked in the xy plane. The velocity magnitude minimum at the diagram for the trajectory with the 80 degrees angle is 3.82 m/s. The velocity increases to the certain amount due to the gravity, as a body traveling through a resistive medium.

Figure 12 depicts a decrease of translational kinetic energy for a fragment with a mass of 7.89 g. Translational kinetic energy is defined as half of the product of the mass of the fragment and the square of the intensity of the total translational velocity. Initial translational kinetic energy for 7.89 g fragment was 3.94 kJ. Translational kinetic energy values for the 7.89g fragment, when it hits the ground, are 3-16J for the given elevation angles (not enough to incapacitate human target).

Considering the distance of 50m from the detonation point, significant from the standpoint of estimating the lethal zone of HE projectile, then the translational kinetic energy for this fragment (at a distance of 50m from the center of the explosion ranges) ranges from 1.5 kJ for elevation angle 5° to about 1,3 kJ for elevation angle 20° (more than enough to incapacitate human target).
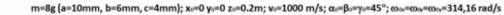

Figure 12. Decrease of translational kinetic energy for a fragment with a mass of 7.89 g for different elevation angles

Although the diagram does not show clearly the increase of the velocity after reaching the top point of every trajectory, it exists in the diagram of the kinetic energy. The expression for kinetic energy has the term v^2, which means that the high values significantly increase, but those near zero velocity (about the highest point of the trajectory) get even smaller, and practically they are not visible in the Fig. 12. The first trajectory (with the highest elevation angle) to the left drops to almost zero at about 40 meters in x direction in Fig. 11. It can be seen that there is a small value of the velocity magnitude around this position in Fig. 11. In similar way, the small value of the velocity that is obtained after the peek point is not clearly visible in Fig. 12 due to the square term. Relatively small values of the kinetic energy can be seen in the logarithmic scale in Fig. 13.
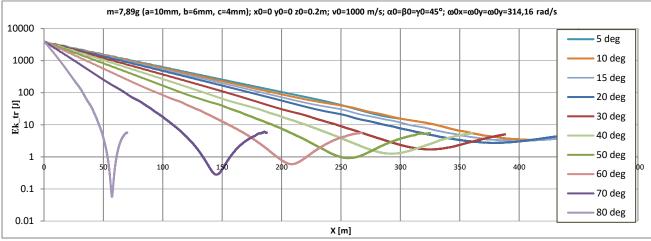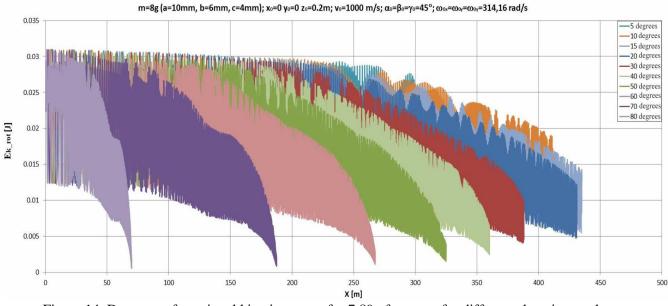
Figure 13. Decrease of translational kinetic energy for a fragment with a mass of 7.89 g for different elevation angles - logarithmic scale
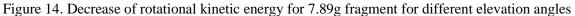
In the analysis, we also evaluated the rotational kinetic energy of the fragments in order to assess its intensity in relation to the intensity of the translational kinetic energy. The rotational kinetic energy of the fragment is defined as half of the product of a moment of inertia of the body (inertia moments in the coordinate system tied to the body are used, which are constant for axes ξ, η and ζ) and a square of the intensity of the total angular velocity of the body.

Figure 14 shows a decrease of rotational kinetic energy for 7.89 g fragment. The initial rotational kinetic energy for this fragment was 0.03 J. The rotational kinetic energy values for the 7.89 g fragment, when it hits the ground, are from 0.00099J to 0.026J for given elevation angles.

As can be seen from the results (Figure 12), the translational kinetic energy of the fragment is much higher than the rotational component of kinetic energy. Thus, the translational kinetic energy of the 7.89 g fragment, for given initial conditions, is 136311 times larger than the rotational kinetic energy at the beginning of the movement, and at the end of the movement it is about 230 times higher (for elevation angle 15°) to 5681 times higher (for elevation angle 80°).

So, as far as the kinetic energy of the body (fragment) is concerned, the kinetic energy of translation is dominant in relation to the kinetic energy of the rotation of the fragment.

Figure 14. Decrease of rotational kinetic energy for 7.89g fragment for different elevation angles

From the point of view of the parameters of the lethal zone of HE projectiles, it is generally important to estimate the trajectory of the fragments in the range up to 50m.

So, using the same fragment (m=7.89g; a=10mm, b=6mm i c=4mm) the influence of the initial translational velocity on a trajectory and kinetic energy were calculated for the following conditions:
- The initial height of the fragment is arbitrarily chosen, $z_0 = 1$m.
- The initial elevation angle of the fragment was equal to zero.
- The vector of the initial translational velocity is set in the positive direction of axis x (see also Fig. 5).
- The initial angular velocity was set to zero. This is an idealized case, but it is useful (for the purpose of isolating translational velocity influence on motion) in this analysis.
- The initial orientation of the fragment, i.e., the initial absolute angles α_0, β_0 and γ_0 were zero, which means that the fragment was in the reference initial position. This is also an idealization (but useful in analysis) because rarely these angles can be zero in the real situation.
- The initial translational velocity were: 1000 m/s, 1200 m/s, 1500 m/s and 2000 m/s.
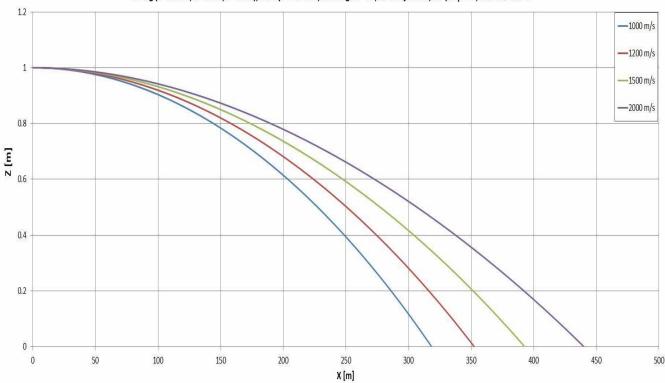
The trajectories obtained are shown in Fig. 15, where it can be clearly seen how initial velocity impacts fragment range and trajectory.

Figure 16 shows a diagram of the change of the kinetic energy for the given fragment (mass of 7.89g) for different initial translational velocities, up to a distance of 50m. The diagrams in Figures 15 and 16 show that the initial velocity of the fragment significantly influences its range, and especially the level of the kinetic energy of the fragment. In the example, for the same fragment (mass of 7.89g), at initial translational velocity of 1000 m/s (i.e. fragments from a 130mm HE M79 artill. projectile), a fragment for the given initial conditions has a range of around 318m and kinetic energy when it hits the ground of 1.1kJ.
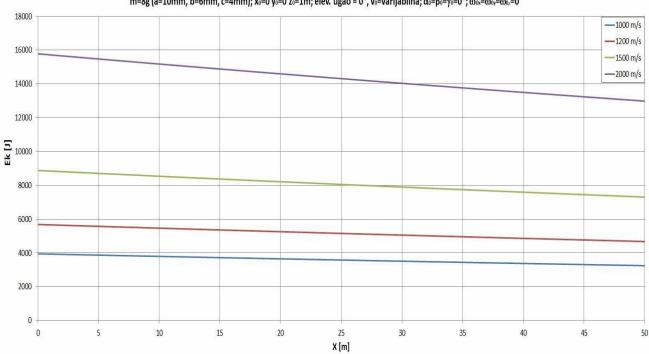
On the other hand, this same fragment, if it has an initial velocity of 2000 m/s (i.e. 128mm HE M87 - Comp. B rocket projectile fragments have similar velocities), has a range of around 440m (28% higher), and kinetic energy when hitting the ground of 2.8 kJ (61% higher than in the case of initial velocity of 1000 m/s).

So, this fragment, for given initial conditions, at a 50m distance will certainly disable an unprotected human target (NATO standard stipulates 80J as incapacitation energy criterion).

Figure 15. Influence of the initial translational velocity on a fragment trajectory

Figure 16. Change of the kinetic energy for the given fragment (mass of 7.89g) for different initial translational velocities, up to a distance of 50m.

5.   Conclusion

A generalized (6DOF) model for evaluating fragment trajectory elements is defined, which incorporates a novel model for estimating the projected surface of the body and novel model for estimating aerodynamic force and moment. This 6DOF model is developed on the basis of differential equations of the center of mass motion and movement around the center of mass, and can model the parameters that play an essential role in movement of the bodies with irregular shape through the atmosphere. In our model the basic parameters (i.e. body dimensions) can be arbitrarily changed in the initial part of the analysis, and based on their values and values of initial kinematic parameters (initial velocity, position, orientation), trajectories can be determined (as well as other parameters: velocities, orientation) in a relatively short amount of time.

This model could also be potentially used wherever there is a need to calculate flight mechanics parameters of irregularly shaped bodies. Generalized (6DOF) model for estimation of an irregularly shaped body trajectory is implemented in a new computer program, written in MatLab.

Based on the model, the trajectory calculations were performed for the complete trajectory and for shorter distances to the center of the explosion, with varied geometric-inertial parameters and initial kinematic conditions for the given fragment.

6. Data availability statement
Some or all data, models, or code that support the findings of this study are available from the corresponding author upon request.

References
[1] L.A. Twisdale and P.J. Wickery, "Comparison of debris trajectory models for explosive safety hazard analysis," *25th DoD Explosive Safety Seminar*, Anaheim, California, 1992.
[2] J. Hokanson, "Fragment and debris hazards from accidental explosions," Naval Surface Weapons Center, Dahlgren VA, 1981.
[3] E.W. Baker, P.S. Westine, J.J. Kulesz, J.S. Wilbeck and P.A. Cox, "Manual for the prediction of blast and fragment loadings on structures," USDOE Albuquerque Operations Office, 1980.

[4] F. McCleskey, "Quantity Distance Fragmenf Hazard Computer Program," Naval Surface Warfare Center, 1988.

[5] L.A. Twisdale, W.L. Dunn and R.A. Frank, "Probabilistic methodology for turbine missile risk analysis," *Nuclear Engineering and Design*, 1984.

[6] J.G. Connor, Jr., "Accidental Torpedo Detonation in Submarine Tender Workshops," *Nineteenth Explosives Safety Seminar*, Los Angeles, CA, 1980.

[7] M.M. Swisdak, Jr., "Determination of Safe Handling Arcs Around Nuclear Attack Submarines," *Nineteenth Explosives Safety Seminar*, Los Angeles, CA, 1980.

[8] M. Crull and M.M. Swisdak, Jr., "Methodologies for calculating primary fragment characteristics," Department of Defense Explosives Safety Board, Alexandria, VA, 2005.

[9] H.L. Schreyer and L.E. Romesberg, "Analytical Model for High Explosive Munitions Storages," Mechanics Research Inc., Albuquerque, NM, 1970.

[10] W.E. Baker W. E., J.J. Kulesz, R.E. Ricker, P.S. Westine, V.B. Parr, L.M. Vargas and P.K. Moseley, "Workbook for Estimating Effects of Accidental Explosions in Propellant Ground Handling and Transport Systems," NASA Contractor Report 3023, 1978.

[11] S. Murman, "Characterization of space shuttle ascent debris aerodynamics using CFD methods," *43rd AIAA Sciences Meeting*, 2005.

[12] J.F. Moxnes, Ø. Frøyland, J. Ivar, I.J. Øye, T.I. Brate, E. Friis, G. Ødegårdstuen, T.H. Risdal, "Projected area and drag coefficient of high velocity irregular fragments that rotate or tumble," *Defence Technology*, 2017.

[13] TNO Report, "General description of the missile systems damage assessment code (MISDAC)," Prins Maurits Laboratorium TNO, 1994.

[14] E. Kljuno and A. Catovic, "Estimation of projected surface area of irregularly shaped fragments," *Defence Technology Journal*, 2019a.

[15] E. Kljuno and A. Catovic, "A generalized model for estimation of aerodynamic forces and moments for an arbitrary shaped body," *Defence Technology Journal*, 2019b.

[16] B. Zecevic, J. Terzic, A. Catovic and S. Serdarevic-Kadic, "Influencing parameters on HE projectiles with natural fragmentation," *New Trends in Research of Energetic Materials*, Pardubice, 2006.

[17] A. Catovic and E. Kljuno, "Prediction of aerodynamic coefficients for irregularly shaped body using numerical simulations," *International Journal of Advanced and Applied Sciences*, 5(7), Pages: 71-85, 2018.